

On-the-fly ab initio semiclassical evaluation of absorption spectra of polyatomic molecules beyond the Condon approximation

Aurélien Patoz, Tomislav Begušić, and Jiří Vaníček*

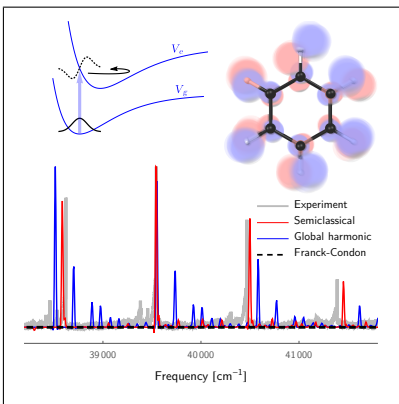
*Laboratory of Theoretical Physical Chemistry, Institut des Sciences et Ingénierie Chimiques,
Ecole Polytechnique Fédérale de Lausanne (EPFL), CH-1015, Lausanne, Switzerland*

E-mail: jiri.vanicek@epfl.ch.

Abstract

To evaluate vibronic spectra beyond the Condon approximation, we extend the on-the-fly *ab initio* thawed Gaussian approximation by considering the Herzberg-Teller contribution due to the dependence of the electronic transition dipole moment on nuclear coordinates. The extended thawed Gaussian approximation is tested on electronic absorption spectra of phenyl radical and benzene: Calculated spectra reproduce experimental data and are much more accurate than standard global harmonic approaches, confirming the significance of anharmonicity. Moreover, the extended method provides a tool to quantify the Herzberg-Teller contribution: we show that in phenyl radical, anharmonicity outweighs the Herzberg-Teller contribution, whereas in benzene, the Herzberg-Teller contribution is essential, since the transition is electronically forbidden and Condon approximation yields a zero spectrum. Surprisingly, both adiabatic harmonic spectra outperform those of the vertical harmonic model, which describes the Franck-Condon region better. Finally, we provide a simple recipe for orientationally averaging spectra, valid beyond Condon approximation, and a relation among the transition dipole, its gradient, and nonadiabatic coupling vectors.

Graphical TOC Entry



Vibrationally resolved electronic spectroscopy provides a valuable insight into the structure and dynamics of polyatomic molecules.¹ Indeed, light-induced molecular dynamics is recognized as one of the key areas of research in physical chemistry, not only for fundamental understanding of Nature, but also for various applications, from solar cells to photodynamic therapy.² The development of theoretical methods for simulating and understanding optical spectra is, therefore, of great importance.

The time-dependent approach to spectroscopy³ evaluates the vibronic spectrum as the Fourier transform of the nuclear wavepacket autocorrelation function, and, in contrast to the commonly used time-independent Franck-Condon approach,^{4,5} can easily account for effects beyond the Born-Oppenheimer and global harmonic approximations. In the time-dependent approach, one must first perform exact or approximate molecular quantum dynamics. While the exact quantum dynamics typically requires a global potential energy surface^{6,7} and thus scales exponentially with dimensions, semiclassical methods, such as the initial value representation,⁸ thawed Gaussian approximation (TGA),⁹ frozen Gaussian approximation,¹⁰ and Herman-Kluk propagator^{11,12} require only local information and are suitable for on-the-fly implementation. The idea of using multiple frozen Gaussians as a basis for describing the full wavepacket has inspired a number of quantum¹³⁻¹⁵ and semiclassical¹⁶⁻²¹ “first-principles” approaches, which allow a combination with an on-the-fly *ab initio* (OTF-AI) evaluation of the electronic structure. Apart from a few examples,²² thawed Gaussians have been largely marginalized since they can neither describe wavepacket splitting nor very anharmonic dynamics. Yet, vibrationally resolved electronic spectra are mostly determined by short-time dynamics, during which both wavepacket splitting and anharmonic effects are less important. Indeed, a recent implementation of an on-the-fly *ab initio* thawed Gaussian approximation (OTF-AI-TGA) reproduced successfully vibrational structure of electronic absorption, emission, and photoelectron spectra, even in rather anharmonic and floppy systems such as ammonia.^{23,24}

Here, an extension of the OTF-AI-TGA beyond the Condon approximation is presented

by employing the Herzberg-Teller (HT) approximation,²⁵ which, in contrast to the Condon approximation,⁴ includes a linear dependence of the transition dipole moment on nuclear coordinates. We employ the OTF-AI implementation of the extended thawed Gaussian approximation (ETGA)²⁶ to evaluate the absorption spectra of phenyl radical, an anharmonic system allegedly exhibiting a significant Herzberg-Teller contribution,²⁷ and benzene, a textbook example of a symmetry-forbidden (i.e., electronically forbidden) transition.²⁸

At zero temperature, within the electric-dipole approximation, first-order time-dependent perturbation theory, and rotating-wave approximation, the absorption cross section of a molecule with two electronic states that are not nonadiabatically coupled can be expressed as the Fourier transform

$$\sigma_{\mu\mu}(\omega) = \frac{2\pi\omega}{\hbar c} \int_{-\infty}^{\infty} C_{\mu\mu}(t) e^{i\omega t} dt \quad (1)$$

of the dipole time autocorrelation function

$$C_{\mu\mu}(t) = \langle 1, g | e^{i\hat{H}_1 t/\hbar} \hat{\mu} e^{-i\hat{H}_2 t/\hbar} \hat{\mu} | 1, g \rangle = \langle \phi(0) | \phi(t) \rangle e^{-iE_{1,g}t/\hbar}, \quad (2)$$

where \hat{H}_1 and \hat{H}_2 are nuclear Hamiltonian operators of the ground and excited electronic states, $\hat{\mu}$ is the matrix element $\hat{\mu} (= \hat{\mu}_{21})^1$ of the electric transition dipole moment operator projected along the polarization unit vector $\vec{\epsilon}$, i.e., $\hat{\mu} := \hat{\vec{\mu}} \cdot \vec{\epsilon}$, and $|1, g\rangle$ is the ground vibrational state of the ground electronic state with zero-point energy $E_{1,g}$. Thus, the vibronic spectrum can be evaluated by propagating the initial wavepacket $|\phi(0)\rangle = \hat{\mu}|1, g\rangle$ on the excited state potential energy surface.

To compare with an experiment in gas phase, where the molecules are isotropically distributed, one must average the computed spectrum over all molecular orientations. Yet, due to the isotropy of space, a brute-force numerical averaging is avoided; averaging is required only over three orientations of the molecule.²⁹ To show this, consider the spectrum and autocorrelation function as 3×3 tensors $\sigma_{\vec{\mu}\vec{\mu}}(\omega)$ and $C_{\vec{\mu}\vec{\mu}}(t)$, the latter related to $C_{\mu\mu}(t)$ by

¹The subscript 21 is removed for simplicity since we will almost exclusively consider this matrix element.

$C_{\mu\mu}(t) = \vec{\epsilon}^\top \cdot C_{\vec{\mu}\vec{\mu}}(t) \cdot \vec{\epsilon}$. A simple analytical calculation³⁰ shows that the average over all orientations of the polarization vector $\vec{\epsilon}$ is $\overline{C_{\mu\mu}(t)} = (1/3)\text{Tr}[C_{\vec{\mu}\vec{\mu}}(t)]$ and the corresponding absorption cross section is

$$\overline{\sigma(\omega)} = \frac{1}{3}\text{Tr}[\sigma_{\vec{\mu}\vec{\mu}}(\omega)] = \frac{1}{3}(\sigma_{\mu_x\mu_x} + \sigma_{\mu_y\mu_y} + \sigma_{\mu_z\mu_z}). \quad (3)$$

Thus, the average is easily evaluated, e.g., by averaging over only three arbitrary orthogonal molecular orientations with respect to the fixed polarization vector $\vec{\epsilon}$ or by fixing the molecular orientation and averaging over only three arbitrary orthogonal polarization vectors.

While the result (3) holds for arbitrary coordinate dependence of the transition dipole $\vec{\mu}(q)$, two approximations are frequently used. Within the most common Condon approximation, the transition dipole is considered constant: $\vec{\mu}(q) \approx \vec{\mu}(q_0)$ and the general result (3) reduces to the textbook recipe for the averaged Franck-Condon (FC) spectrum:

$$\overline{\sigma_{\text{FC}}(\omega)} = \frac{1}{3}\sigma_{|\vec{\mu}||\vec{\mu}|}(\omega). \quad (4)$$

(“Divide by 3 the spectrum for the molecular dipole aligned with the field.”) In the more accurate Herzberg-Teller approximation, the transition dipole moment becomes a linear function of nuclear coordinates:

$$\vec{\mu}(q) \approx \vec{\mu}(q_0) + \text{grad}_q \vec{\mu}|_{q_0}^\top \cdot (q - q_0) \quad (5)$$

By explicitly differentiating the matrix element $\vec{\mu}_{\alpha\beta}$ of the molecular dipole between electronic states α and β (for a moment we reintroduce the subscripts), one can show³⁰ that

$$\frac{\partial}{\partial q_i} \vec{\mu}_{\alpha\beta} = \sum_{\gamma} (\vec{\mu}_{\alpha\gamma} F_{i,\gamma\beta} - F_{i,\alpha\gamma} \vec{\mu}_{\gamma\beta}) + \left(e \sum_{j=1}^N Z_j \frac{\partial \vec{R}_j}{\partial q_i} \right) \delta_{\alpha\beta}, \quad (6)$$

or, in a more compact matrix notation:

$$\frac{\partial}{\partial q_i} \vec{\mu} = [\vec{\mu}, \mathbf{F}_i] + \left(e \sum_{j=1}^N Z_j \frac{\partial \vec{R}_j}{\partial q_i} \right) \mathbf{1}, \quad (7)$$

where N is the number of atoms, Z_j the atomic number and \vec{R}_j the coordinates of the j th atom, and $F_{i,\alpha\beta} := \langle \alpha | (\partial \beta / \partial q_i) \rangle$ is the i th component of the nonadiabatic coupling vector between states α and β . For the *transition* dipole moment, $\alpha \neq \beta$ and the term proportional to $\delta_{\alpha\beta}$ in Eq. (6) [to $\mathbf{1}$ in Eq. (7)] vanishes, which shows that the Herzberg-Teller dependence originates from a combination of nonzero nonadiabatic and dipole couplings of states α and β to an intermediate state γ . Moreover, since one may usually neglect nonadiabatic couplings between the ground and excited electronic states at the ground state optimized geometry, only the second term of the commutator survives:

$$\frac{\partial}{\partial q_j} \vec{\mu}_{21} \approx - \sum_{\gamma} F_{i,2\gamma} \vec{\mu}_{\gamma 1}, \quad (8)$$

showing that a nonvanishing gradient of the transition dipole between the ground state 1 and excited state 2 requires an intermediate, “bright” ($\vec{\mu}_{\gamma 1} \neq 0$) excited state γ that is vibronically coupled ($F_{i,2\gamma} \neq 0$) to the excited state 2. Such interpretation reveals the deep connection between the Herzberg-Teller approximation and the concepts of “vibronic coupling” and “intensity-borrowing.”³¹ Finally, although Eq. (7) suggests a way to evaluate $\partial_q \vec{\mu}_{\alpha\beta}$ from $\vec{\mu}$ and \mathbf{F}_i , it is usually easier to evaluate the gradient by finite difference.

To find the autocorrelation function $C_{\mu\mu}(t)$, one must propagate the wavepacket. Heller’s TGA^{3,9,26} relies on the fact that a Gaussian wavepacket evolved in at most quadratic potential remains a Gaussian. Within this approximation, the anharmonicity of the potential is taken into account partially by propagating the Gaussian wavepacket

$$\psi_t(q) = N_0 \exp \left\{ -(q - q_t)^\top \cdot A_t \cdot (q - q_t) + \frac{i}{\hbar} [p_t^\top \cdot (q - q_t) + \gamma_t] \right\} \quad (9)$$

in the time-dependent effective potential given by the local harmonic approximation of the full potential

$$V_{\text{eff}}(q, t) = V|_{q_t} + (\text{grad}_q V|_{q_t})^\top \cdot (q - q_t) + \frac{1}{2}(q - q_t)^\top \cdot \text{Hess}_q V|_{q_t} \cdot (q - q_t), \quad (10)$$

where $V|_{q_t}$, $\text{grad}_q V|_{q_t}$, and $\text{Hess}_q V|_{q_t}$ denote the potential energy, gradient, and Hessian evaluated at the center of the Gaussian, N_0 is the initial normalization constant, (q_t, p_t) are the phase-space coordinates of the center of the Gaussian wavepacket at time t , A_t is the complex symmetric width matrix, and γ_t is a complex number; its real part gives an overall phase factor and its imaginary part ensures the normalization of the Gaussian wavepacket at all times. Parameters of the Gaussian follow Heller's equations of motion^{3,9,26}

$$\dot{q}_t = m^{-1} \cdot p_t \quad (11)$$

$$\dot{p}_t = -\text{grad}_q V|_{q_t} \quad (12)$$

$$\dot{A}_t = -2i\hbar A_t \cdot m^{-1} \cdot A_t + \frac{i}{2\hbar} \text{Hess}_q V|_{q_t} \quad (13)$$

$$\dot{\gamma}_t = L_t - \hbar^2 \text{Tr}(m^{-1} \cdot A_t), \quad (14)$$

where m is the diagonal mass matrix and L_t the Lagrangian.

The extended TGA used in this work considers a more general form of the initial wavepacket, namely a Gaussian wavepacket (9) multiplied by a polynomial $P(q - q_0)$ in nuclear coordinates, which, at time zero, can be written as a polynomial in the derivatives with respect to p_0 :

$$\phi_0(q) = P(q - q_0) \psi_0(q) = P\left(\frac{\hbar}{i} \frac{\partial}{\partial p_0}\right) \psi_0(q). \quad (15)$$

This observation leads to a simple recipe for propagating the extended TGA wavepacket within the local harmonic approximation;²⁶ namely, the wavepacket retains this form at all times:

$$\phi_t(q) = P\left(\frac{\hbar}{i} \frac{\partial}{\partial p_0}\right) \psi_t(q), \quad (16)$$

where $\psi_t(q)$ is the original TGA wavepacket (9). As for the initial Herzberg-Teller wavepacket, $P(q - q_0) = \mu(q_0) + b_0^\top \cdot (q - q_0)$, where $b_0 = \text{grad}_q \mu|_{q_0}$, and the semiclassical propagation yields

$$\phi_t(q) = [\mu(q_0) + b_t^\top \cdot (q - q_t)] \psi_t(q). \quad (17)$$

The four parameters of the Gaussian $\psi_t(q)$ are propagated with the usual TGA equations (11)-(14) and only one additional parameter, b_t , must be evaluated:

$$b_t = (-2i\hbar A_t \cdot M_{qp,t} + M_{pp,t}) \cdot b_0, \quad (18)$$

where $M_{qp,t} = \partial q_t / \partial p_0$ and $M_{pp,t} = \partial p_t / \partial p_0$ are the elements of the stability matrix, which is already needed for propagating A_t and γ_t , implying that the additional evaluation of b_t comes at almost no additional cost. Remarkably, the orientational averaging of ETGA spectra is even simpler than what could be expected from the general simplification we mentioned in the beginning: within ETGA, the averaging requires only a single trajectory (instead of three) because the transition dipole moment does not affect the propagation of q_t , p_t , A_t , γ_t .

As a consequence of this property, the ETGA can be combined with an on-the-fly *ab initio* scheme at the same cost as the original TGA for spectra within Condon approximation.^{23,24} The *ab initio* calculations are typically performed in Cartesian coordinates, and therefore the *ab initio* gradients and Hessians needed in Eq. (10) must be transformed^{23,24} to the coordinate system q that fits into our framework—the vibrational normal modes.

As the extended TGA is exact in a globally harmonic potential, it is useful to compare the on-the-fly approach with two common approximations of the excited-state potential energy surface: the vertical harmonic (VH) and adiabatic harmonic (AH) approximations,³² in which the excited-state potential is expanded to the second order about the ground and excited state optimized geometries, respectively (see Refs. 23 and 24 for details). We use density functional theory for the ground and time-dependent density functional theory for the excited state *ab initio* calculations; B3LYP/SNSD for phenyl radical and B3LYP/6-

31+G(d,p) for benzene (see Supporting Information for details and validation by comparison with a higher level *ab initio* method).

According to Barone and coworkers,^{27,33} the calculation of the absorption spectrum corresponding to $\tilde{A}^2B_1 \leftarrow \tilde{X}^2A_1$ electronic transition of phenyl radical depends on the dimensionality of the simulation model and on the inclusion of the Herzberg-Teller contribution, anharmonicity effects, and mode-mixing (Duschinsky effect).³⁴ Our model includes all these effects and provides the means to evaluate their importance.

To assess the influence of anharmonicity, the experimental spectrum is compared with the spectra simulated using the global harmonic approaches (Fig. 1, top). While the vertical harmonic approach only captures the overall envelope of the experimental spectrum, but fails to capture any details, the adiabatic harmonic model reproduces all main features of the spectrum. This is in contrast with the common expectation that the vertical harmonic approach should be more accurate,^{32,35} as it describes better the Franck-Condon region of the excited state potential. Indeed, the emission spectra of oligothiophenes²³ and both absorption and photoelectron spectra of ammonia²⁴ are much better described with the VH than the AH approach. In phenyl radical, the failure of the VH approach lies in the incorrect frequencies and displacements of the two most displaced modes 18 and 24 (Fig. S4 of Supporting Information), resulting in the missing mode effect:^{36,37} when the spectrum is not well resolved, it may contain a single progression whose spacing does not correspond to any of the vibrational frequencies of the system. Unlike the global harmonic approaches, the on-the-fly method overcomes the problem of guessing which excited state Hessian should be used (i.e., vertical or adiabatic) and reproduces the experimental spectrum rather well; moreover, with minimum human input.

To assess the validity of the Condon approximation, the FC and Franck-Condon Herzberg-Teller (FCHT) spectra of phenyl radical are compared at the bottom of Fig. 1. The FC and FCHT spectra are very similar since the absorption spectrum of phenyl radical is mostly determined by the symmetry-allowed Franck-Condon transition, while the Herzberg-Teller

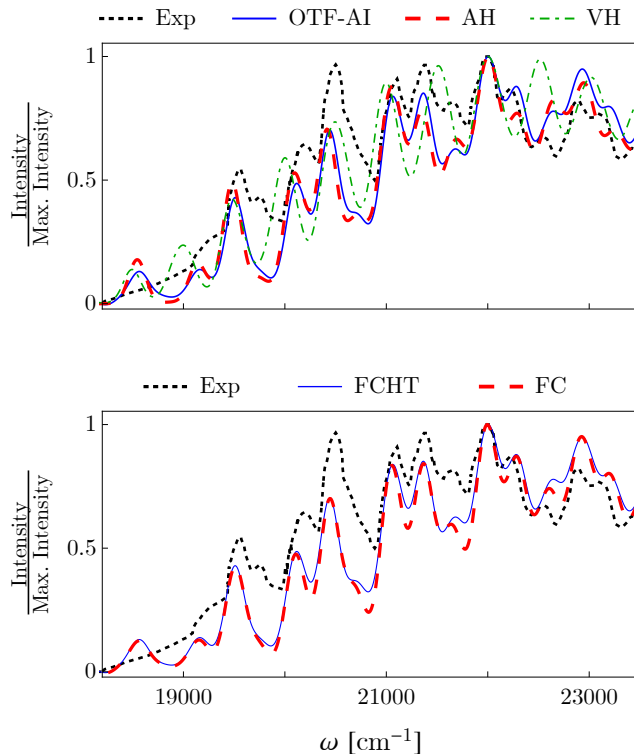


Figure 1: Calculated absorption spectra of phenyl radical $\tilde{A}^2B_1 \leftarrow \tilde{X}^2A_1$ electronic transition compared to the experimental^{33,38} spectrum measured in Ar matrix at 6 K. Top: Comparison of the on-the-fly *ab initio* extended TGA (OTF-AI-ETGA), adiabatic harmonic (AH), and vertical harmonic (VH) models (all using the FCHT approximation). Bottom: Comparison of the Franck-Condon (FC) and Franck-Condon Herzberg-Teller (FCHT) approximations (both evaluated with OTF-AI-ETGA). All spectra are horizontally shifted and rescaled according to the highest peak (see Table S7 of Supporting Information).

contribution only broadens the peaks slightly. We find that, in phenyl radical, including anharmonicity effects with the OTF-AI scheme is more important than including the HT contribution with the extension of the TGA.

Both the ground and excited state geometries of benzene belong to the D_{6h} point group. Group theory predicts that the $\tilde{A}^1B_{2u} \leftarrow \tilde{X}^1A_{1g}$ electronic transition is symmetry-forbidden. Yet it is vibronically allowed, since the nonzero elements of the gradient of the transition dipole moment give rise to the vibronic spectrum.²⁸ The gradient of the transition dipole moment originates mostly from nonadiabatic couplings between the B_{2u} state and the bright E_{1u} state.³⁹ The spectrum contains one strong progression, assigned to one of the totally symmetric modes, as well as a number of hot bands. At present we do not attempt to simulate the hot bands, which require a finite-temperature treatment;⁴⁰ our goal is computing the correct absorption cross sections of the main progression. In addition, we do not treat the spectral features arising from the second order vibronic coupling, i.e., a number of small intensity peaks which cannot be described within the first-order Herzberg-Teller approximation.⁴¹

Interestingly, the adiabatic harmonic approach again reproduces the experimental spectrum at least qualitatively, unlike the vertical harmonic approach which results in a number of peaks not observed in the experiment (Fig. 2, top). In the VH model, modes 25, 29 and 30 are more distorted since their frequencies are significantly lower than the corresponding frequencies in the AH model (see Table S6 and Fig. S5 of Supporting Information). Again, due to a partial treatment of anharmonicity, the OTF-AI-ETGA spectrum shows significant improvement over both global harmonic methods: While the relative intensities of AH peaks have errors of 20 to 50% and the VH model fails completely, the relative intensities of the OTF-AI-ETGA peaks lie within 5% of experiment. Influence of anharmonicity on the spectrum is investigated using the autocorrelation functions in Supporting Information (see Figs. S6–S8). To further explore whether it is the error in the phase or magnitude of the autocorrelation function that affects the spectra more, we construct two hybrid, nonphysical

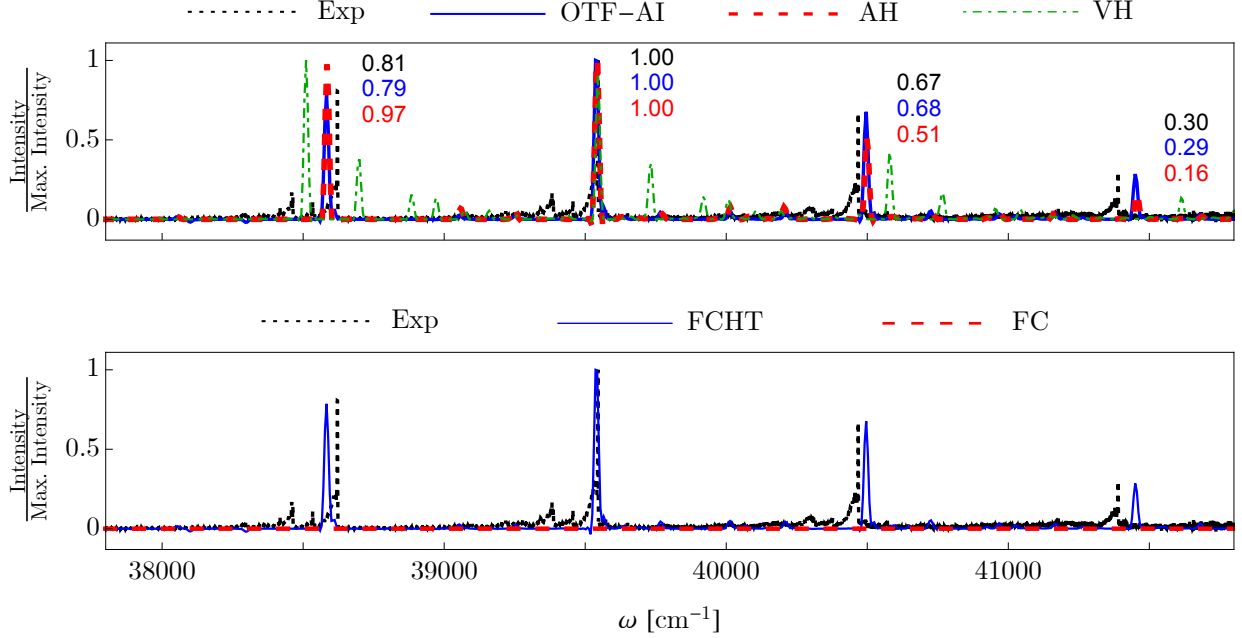


Figure 2: Calculated absorption spectra of benzene $\tilde{A}^1B_{2u} \leftarrow \tilde{X}^1A_{1g}$ electronic transition compared to the experimental^{42,43} spectrum measured at 293 K. See the caption of Fig. 1 for details. To clarify the difference between the adiabatic harmonic (AH, red) and on-the-fly (blue) spectra, we show the scaled intensities of the experimental, AH, and on-the-fly peaks.

autocorrelation functions. The first, denoted $|AH| \exp(i \text{OTF})$, combines the magnitude of the adiabatic harmonic autocorrelation function with the phase from the on-the-fly correlation function, while the second, denoted $|\text{OTF}| \exp(i AH)$, combines the magnitude of the on-the-fly autocorrelation function with the phase from the adiabatic harmonic autocorrelation function. The spectra in Fig. 3 simulated using these two hybrid autocorrelations show clearly that it is the error in the phase of the AH model that most corrupts the intensities of the peaks. The difference between the two phases is closely related to the propagation of the stability matrix, and, consequently, to the Hessians of the excited electronic state potential.

In contrast to almost perfect description of the intensities by the OTF-AI-ETGA, neither the AH nor the OTF-AI-ETGA reproduces correctly the experimental spacing of the peaks in the main progression. This error, however, can be assigned to the electronic structure method, implying that the use of other density functional or wavefunction-based methods could give more accurate curvature of the potential, and hence a better spacing.

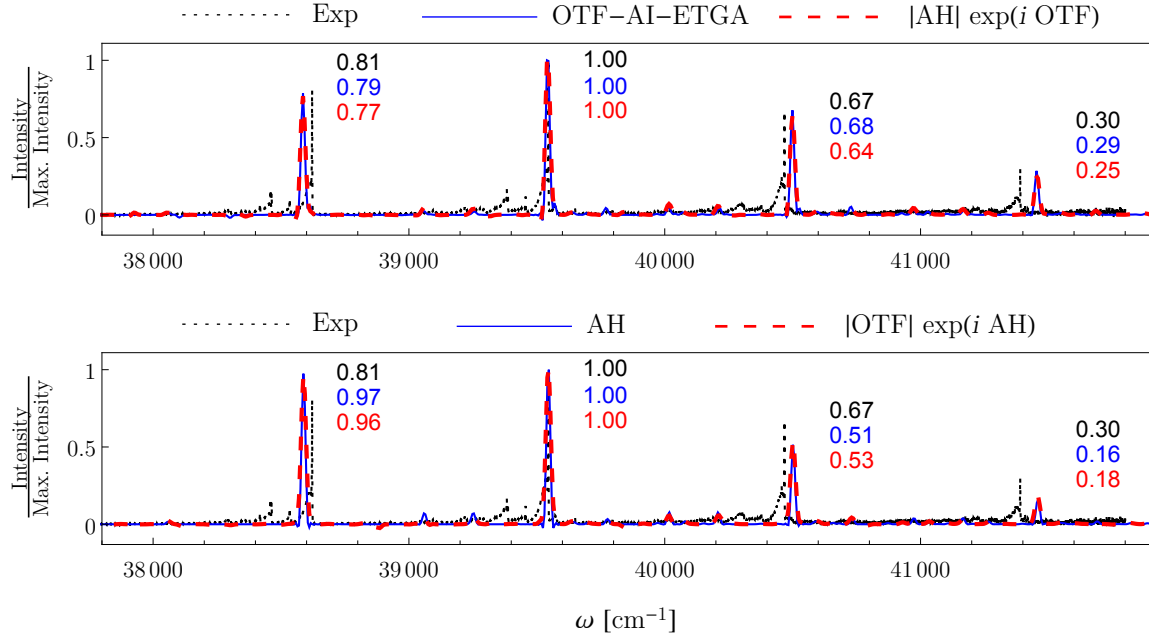


Figure 3: Spectra calculated from the hybrid autocorrelation functions: the $|AH| \exp(i \text{OTF})$ spectrum is almost the same as the very accurate OTF-AI-ETGA spectrum (top), while the $|OTF| \exp(i \text{AH})$ spectrum overlaps with the less accurate adiabatic harmonic spectrum (bottom), confirming that the error in the phase of the autocorrelation function is more important than the error in its magnitude (see Table S7 of Supporting Information). Scaled peak intensities are shown as in Fig. 2.

Our main result is contained in the bottom panel of Fig. 2, which compares the Franck-Condon spectrum (based on the Condon approximation), which can be evaluated with the original TGA, and the FCHT spectrum (based on the Herzberg-Teller approximation), which requires the extended TGA. While the FCHT agrees very well with experiment, the Franck-Condon spectrum is zero, since the transition dipole moment at the ground-state equilibrium is zero, which is the precise meaning of an electronically forbidden transition.

Incidentally, one can imagine simulating the FC spectrum by the commonly adopted procedure in which the transition dipole moment is set to unity and the spectrum is rescaled at the end. Although reasonable for electronically allowed transitions, here this “blind” procedure makes no sense since $\mu_{\text{FC}} = 0$. This “FC” approach is compared to the FCHT result (see Fig. S9 of Supporting Information), and, somewhat surprisingly, the spectra are very similar, the main difference being a constant shift corresponding exactly to the excited state frequency of the degenerate inducing modes 27 and 28 (see Tables S5–S6 of Supporting Information). However, such similarity between the “FC” and the FCHT approach is not general. In addition, the “FC” approach is not capable of reproducing the *absolute* magnitudes of absorption cross sections, while the full FCHT approach provides a good estimate of the absolute absorption cross sections, as shown in Fig. S10 of Supporting Information.

To conclude, we presented an extension to the on-the-fly *ab initio* TGA and employed it to evaluate absorption spectra of phenyl radical and benzene within the Herzberg-Teller approximation. Considerable improvement compared to the usual global harmonic approaches was achieved and a further insight into the origins of the spectral features was given. The results obtained for the absorption spectrum of phenyl radical imply that including the anharmonicity effects is more important than the Herzberg-Teller contribution to the spectrum. Although thawed Gaussian approximation is often described in the context of calculating low-resolution spectra, here we reported the evaluation of a rather high-resolution absorption spectrum of benzene with high accuracy. The improvement was especially pronounced in the intensities of the peaks, due to a partial inclusion of the anharmonicity of the excited state

potential. Thus, the OTF-AI-ETGA can be used not only to reproduce spectra, but more importantly, to evaluate the importance of different effects by going beyond the commonly used Condon and global harmonic approximations.

Supporting Information Available

The following files are available free of charge. Computational details, ground and excited state optimized geometries, transition dipole moments, frequencies, and displacements, validation of the Born-Oppenheimer approximation and of the choice of the electronic structure method, conservation of the phase space volume and symplectic structure, details of spectra calculations, models describing the failure of the vertical harmonic method for absorption spectra, discussion of anharmonicity effects in benzene, “Franck-Condon” (“FC”) spectrum, and absolute absorption cross sections of benzene.

Acknowledgement

The authors acknowledge the financial support from the Swiss National Science Foundation through the NCCR MUST (Molecular Ultrafast Science and Technology) Network, from the European Research Council (ERC) under the European Union’s Horizon 2020 research and innovation programme (grant agreement No. 683069 – MOLEQULE), and from the EPFL.

References

- (1) Herzberg, G. *Atomic Spectra and Atomic Structure*; Dover Publications, 1944.
- (2) Albini, A.; Fasani, E. Introduction and Review of the Year 2015. *Photochemistry* **2016**, *44*, 1–15.

- (3) Heller, E. J. The Semiclassical Way to Molecular Spectroscopy. *Acc. Chem. Res.* **1981**, *14*, 368–375.
- (4) Condon, E. A Theory of Intensity Distribution in Band Systems. *Phys. Rev.* **1926**, *28*, 1182–1201.
- (5) Franck, J.; Dymond, E. G. Elementary Processes of Photochemical Reactions. *Trans. Faraday Soc.* **1926**, *21*, 536–542.
- (6) Meyer, H.-D.; Gatti, F.; Worth, G. A. *Multidimensional Quantum Dynamics: MCTDH Theory and Applications*; WILEY-VCH, 2009.
- (7) Gatti, F. *Molecular Quantum Dynamics - From Theory to Applications*; Springer-Verlag, 2014.
- (8) Miller, W. H. Classical S Matrix: Numerical Application to Inelastic Collisions. *J. Chem. Phys.* **1970**, *53*, 3578.
- (9) Heller, E. J. Time-dependent Approach to Semiclassical Dynamics. *J. Chem. Phys.* **1975**, *62*, 1544–1555.
- (10) Heller, E. J. Frozen Gaussians: A Very Simple Semiclassical Approximation. *J. Chem. Phys.* **1981**, *75*, 2923–2931.
- (11) Herman, M. F.; Kluk, E. A Semiclassical Justification for the Use of Non-spreading Wavepackets in Dynamics Calculations. *Chem. Phys.* **1984**, *91*, 27–34.
- (12) Kay, K. G. Semiclassical Initial Value Treatments of Atoms and Molecules. *Annu. Rev. Phys. Chem.* **2005**, *56*, 255–280.
- (13) Ben-Nun, M.; Quenneville, J.; Martínez, T. J. Ab Initio Multiple Spawning: Photochemistry from First Principles Quantum Molecular Dynamics. *J. Phys. Chem. A* **2000**, *104*, 5161–5175.

- (14) Saita, K.; Shalashilin, D. V. On-the-fly ab initio molecular dynamics with multiconfigurational Ehrenfest method. *J. Chem. Phys.* **2012**, *137*, 22A506.
- (15) Richings, G.; Polyak, I.; Spinlove, K.; Worth, G.; Burghardt, I.; Lasorne, B. Quantum Dynamics Simulations Using Gaussian Wavepackets: the vMCG Method. *Int. Rev. Phys. Chem.* **2015**, *34*, 269–308.
- (16) Tatchen, J.; Pollak, E. Semiclassical On-the-fly Computation of the $S_0 \rightarrow S_1$ Absorption Spectrum of Formaldehyde. *J. Chem. Phys.* **2009**, *130*, 041103.
- (17) Ceotto, M.; Atahan, S.; Shim, S.; Tantardini, G. F.; Aspuru-Guzik, A. First-principles Semiclassical Initial Value Representation Molecular Dynamics. *Phys. Chem. Chem. Phys.* **2009**, *11*, 3861–3867.
- (18) Ceotto, M.; Atahan, S.; Tantardini, G. F.; Aspuru-Guzik, A. Multiple Coherent States for First-principles Semiclassical Initial Value Representation Molecular Dynamics. *J. Chem. Phys.* **2009**, *130*, 234113.
- (19) Wong, S. Y. Y.; Benoit, D. M.; Lewerenz, M.; Brown, A.; Roy, P.-N. Determination of Molecular Vibrational State Energies Using the Ab Initio Semiclassical Initial Value Representation: Application to Formaldehyde. *J. Chem. Phys.* **2011**, *134*, 094110.
- (20) Ianconescu, R.; Tatchen, J.; Pollak, E. On-the-fly Semiclassical Study of Internal Conversion Rates of Formaldehyde. *J. Chem. Phys.* **2013**, *139*, 154311.
- (21) Gabas, F.; Conte, R.; Ceotto, M. On-the-fly Ab Initio Semiclassical Calculation of Glycine Vibrational Spectrum. *J. Chem. Theory Comput.* **2017**, *13*, 2378.
- (22) Grossmann, F. A Semiclassical Hybrid Approach to Many Particle Quantum Dynamics. *J. Chem. Phys.* **2006**, *125*, 014111.

- (23) Wehrle, M.; Šulc, M.; Vaníček, J. On-the-fly Ab Initio Semiclassical Dynamics: Identifying Degrees of Freedom Essential for Emission Spectra of Oligothiophenes. *J. Chem. Phys.* **2014**, *140*, 244114.
- (24) Wehrle, M.; Oberli, S.; Vaníček, J. On-the-fly Ab Initio Semiclassical Dynamics of Floppy Molecules: Absorption and Photoelectron Spectra of Ammonia. *J. Phys. Chem. A* **2015**, *119*, 5685.
- (25) Herzberg, G.; Teller, E. Schwingungsstruktur der Elektronenübergänge Bei Mehratomigen Molekülen. *Z. Phys. Chem. B* **1933**, *21*, 410.
- (26) Lee, S.-Y.; Heller, E. J. Exact Time-dependent Wave Packet Propagation: Application to the Photodissociation of Methyl Iodide. *J. Chem. Phys.* **1982**, *76*, 3035–3044.
- (27) Biczysko, M.; Bloino, J.; Barone, V. First Principle Simulation of Vibrationally Resolved $\tilde{A}^2B_1 \leftarrow \tilde{X}^2A_1$ Electronic Transition of Phenyl Radical. *Chem. Phys. Lett.* **2009**, *471*, 143–147.
- (28) Herzberg, G. *Molecular Spectra and Molecular Structure: III. Electronic Spectra of Polyatomic Molecules*; D.Van Nostrand Company Inc., 1966.
- (29) Hein, B.; Kreisbeck, C.; Kramer, T.; Rodríguez, M. Modelling of oscillations in two-dimensional echo-spectra of the Fenna-Matthews-Olson complex. *New J. Phys.* **2012**, *14*, 023018.
- (30) Begušić, T.; Patoz, A.; Vaníček, J. *In preparation*
- (31) Quack, M.; Merkt, F. *Handbook of High-resolution Spectroscopy*; John Wiley & Sons, 2011.
- (32) Domcke, W.; Cederbaum, L. S.; Köppel, H.; VonNiessen, W. A Comparison of Different Approaches to the Calculation of Franck-Condon Factors for Polyatomic Molecules. *Mol. Phys.* **1977**, *34*, 1759–1770.

- (33) Baiardi, A.; Bloino, J.; Barone, V. General Time Dependent Approach to Vibronic Spectroscopy Including Franck-Condon, Herzberg-Teller, and Duschinsky Effects. *J. Chem. Theory Comput.* **2013**, *9*, 4097–4115.
- (34) Duschinsky, F. On the Interpretation of Electronic Spectra of Polyatomic Molecules. *Acta Physicochim. U.R.S.S.* **1937**, *7*, 551–566.
- (35) Cerezo, J.; Zuniga, J.; Requena, A.; Ávila Ferrer, F. J.; Santoro, F. Harmonic Models in Cartesian and Internal Coordinates to Simulate the Absorption Spectra of Carotenoids at Finite Temperatures. *J. Chem. Theory Comput.* **2013**, *9*, 4947–4958.
- (36) Tannor, D. J. *Introduction to Quantum Mechanics*; University Science Books, 2007.
- (37) Tutt, L. W.; Zink, J. I.; Heller, E. J. Simplifying the MIME: A Formula Relating Normal Mode Distortions and Frequencies to the MIME Frequency. *Inorg. Chem.* **1987**, *26*, 2158–2160.
- (38) Radziszewski, J. Electronic Absorption Spectrum of Phenyl Radical. *Chem. Phys. Lett.* **1999**, *301*, 565–570.
- (39) Li, J.; Lin, C.-K.; Li, X. Y.; Zhu, C. Y.; Lin, S. H. Symmetry Forbidden Vibronic Spectra and Internal Conversion in Benzene. *Phys. Chem. Chem. Phys.* **2010**, *12*, 14967–76.
- (40) He, Y.; Pollak, E. Theory of Cooling of Room Temperature Benzene upon Photo-Excitation to the S1 State. *J. Phys. Chem. A* **2001**, *105*, 10961–10966.
- (41) Fischer, G.; Reimers, J.; Ross, I. CNDO-calculation of second order vibronic coupling in the $1B_{2u} - 1A_{1g}$ transition of benzene. *Chem. Phys.* **1981**, *62*, 187–193.
- (42) Fally, S.; Carleer, M.; Vandaele, A. C. UV Fourier Transform Absorption Cross Sections of Benzene, Toluene, Meta-, Ortho-, and Para-Xylene. *J. Quant. Spectrosc. Radiat. Transf.* **2009**, *110*, 766–782.

- (43) Keller-Rudek, H.; Moortgat, G. K.; Sander, R.; Sørensen, R. The MPI-Mainz UV/VIS Spectral Atlas of Gaseous Molecules of Atmospheric Interest. *Earth Syst. Sci. Data* **2013**, *5*, 365–373.

Supporting information for:

**On-the-fly ab initio semiclassical evaluation of
absorption spectra of polyatomic molecules
beyond the Condon approximation**

Aurélien Patoz, Tomislav Begušić, and Jiří Vaníček

*Laboratory of Theoretical Physical Chemistry, Institut des Sciences et Ingénierie Chimiques,
Ecole Polytechnique Fédérale de Lausanne (EPFL), CH-1015, Lausanne, Switzerland*

Computational details

All *ab initio* calculations were performed using GAUSSIAN09^{S1} electronic structure package. Density functional theory and time-dependent density functional theory have been used with the B3LYP functional for ground and excited states, respectively. 6-31+G(d,p) basis set was used for benzene, while for the phenyl radical we used the SNSD basis set—same basis set was used with B3LYP functional in a previous study.^{S2} An in-house code for running OTF-AI classical dynamics was used in combination with GAUSSIAN09 to compute the trajectories for both the phenyl radical and benzene with a time step of 8 a.u. (≈ 0.2 fs). Hessians were then computed at every fourth step of the trajectory (and interpolated in between).^{S3} The OTF-AI trajectories were run for $T \approx 580$ fs (3000 steps) in the case of the phenyl radical and $T \approx 2$ ps (10^4 steps) for benzene. Due to numerical computation of the excited-state Hessians, the computational cost should be roughly $6N$ times larger than the cost of the trajectory calculation (each Hessian calculation consists of $6N$ gradient evaluations), where N is the number of atoms. However, this is relaxed in two ways: the Hessians are not computed at each step of the trajectory and they can be computed in parallel (Hessian information is not needed for the trajectory propagation). As a result, for both the phenyl radical and benzene, the Hessian calculations took approximately as much real time as the *ab initio* trajectory calculation.

The wavepacket propagation was performed in the ground-state mass-scaled normal mode coordinates; the Hessians, forces, and the gradient of the transition dipole moment were transformed from Cartesian to mass-scaled normal mode coordinates by following the prescription explained in detail in Refs. S3 and S4. The initial Gaussian wavepacket was chosen to be the ground vibrational state of the harmonic fit to the ground potential energy surface. Since only a single set of coordinates is used to represent all quantities, there is no need for additional corrections to account for mode-mixing (Duschinsky effect)—mode-mixing is reflected in the non-diagonal elements of the excited-state Hessian matrix represented in the ground-state normal modes.

The gradient of the transition dipole moment was computed using the first-order finite differences scheme with a step of 10^{-2} Å for the phenyl radical and 10^{-4} Å for benzene. For the phenyl radical, larger step was used; at smaller steps the gradient depends significantly on the step size, whereas at larger step sizes, these values vary only very slowly. The dependence is likely to arise from inaccuracy of the transition dipole moments.

Orientational averaging was performed by computing the autocorrelation functions for three orthogonal orientations of the electric field (i.e. by considering three orthogonal elements of the transition dipole moment μ_x , μ_y , and μ_z) and then taking their average. Since it is only the polynomial part of the wavepacket that changes with the transition dipole moment, the Gaussian parameters of the wavepacket—its position, momentum, width, and phase—are not affected when switching the polarization of the electric field; the on-the-fly *ab initio* extended TGA still requires only one classical trajectory. For the phenyl radical, all three elements of the transition dipole moment are non-zero, whereas for benzene, it is only x and y polarizations which give rise to the observed spectra—both the transition dipole moment and its gradient are zero for z polarization. Thus, for benzene, only two correlation functions have to be evaluated for orientational averaging.

The autocorrelation functions were evaluated for positive times and the spectra were computed numerically using the fast Fourier transform. The broadening of the spectra was introduced by damping the autocorrelation functions: for the phenyl radical a Gaussian decay corresponding to a Gaussian broadening of the spectrum with half-width at half-maximum of 100 cm^{-1} was used, while for the well-resolved benzene spectrum, $\Gamma(t) = \cos^2(\frac{\pi t}{2T})$ damping function was used.

Ground- and excited-state optimized geometries, transition dipole moments, frequencies, and displacements

Phenyl radical

Table S1: Optimized geometries (in Å) of ground (\tilde{X}^2A_1) and first excited (\tilde{A}^2B_1) electronic states of the phenyl radical.

	\tilde{X}^2A_1			\tilde{A}^2B_1		
	X	Y	Z	X	Y	Z
C	0.000	1.227	0.772	0.000	1.213	0.734
C	0.000	1.214	-0.632	0.000	1.228	-0.644
C	0.000	0.000	-1.324	0.000	0.000	-1.343
C	0.000	-1.214	-0.632	0.000	-1.228	-0.644
C	0.000	-1.227	0.772	0.000	-1.213	0.734
C	0.000	0.000	1.398	0.000	0.000	1.549
H	0.000	2.163	1.324	0.000	2.169	1.258
H	0.000	-2.154	-1.178	0.000	-2.160	-1.204
H	0.000	-2.163	1.324	0.000	-2.169	1.258
H	0.000	2.154	-1.178	0.000	2.160	-1.204
H	0.000	0.000	-2.410	0.000	0.000	-2.430

Table S2: Derivatives of the transition dipole moment (in atomic units) of the phenyl radical $\tilde{A}^2B_1 \leftarrow \tilde{X}^2A_1$ electronic transition with respect to the mass-scaled normal mode coordinates of the ground electronic state. The transition dipole moment elements evaluated at the ground-state optimized geometry are: $\mu_x = 0.1354$ a.u. = 0.344 D, $\mu_y = \mu_z = 0$.

Mode	Symmetry	$\partial\mu_x/\partial q$	$\partial\mu_y/\partial q$	$\partial\mu_z/\partial q$
1	a ₂	0	0.00131	0
2	b ₁	0	0	0.00207
3	b ₂	0	0	0
4	a ₁	-0.00021	0	0
5	b ₁	0	0	-0.00404
6	b ₁	0	0	0.00231
7	a ₂	0	-0.00026	0
8	b ₁	0	0	-0.00068
9	a ₂	0	0.00124	0
10	a ₁	0.00057	0	0
11	b ₁	0	0	0.00201
12	a ₁	0.00001	0	0
13	a ₁	-0.00017	0	0
14	b ₂	0	0	0
15	b ₂	0	0	0
16	a ₁	0.00000	0	0
17	b ₂	0	0	0
18	b ₂	0	0	0
19	b ₂	0	0	0
20	a ₁	-0.00071	0	0
21	a ₁	0.00050	0	0
22	b ₂	0	0	0
23	a ₁	0.00024	0	0
24	b ₂	0	0	0
25	a ₁	0.00041	0	0
26	b ₂	0	0	0
27	a ₁	0.00028	0	0

Table S3: Normal modes of the phenyl radical ground electronic state with corresponding frequencies (in cm^{-1}). The excited-state frequencies ω computed at the optimized ground-state geometry [vertical harmonic (VH) model] and optimized excited-state geometry [adiabatic harmonic (AH) model] are given in cm^{-1} . The displacements δ between the minima of the ground and excited state global harmonic potentials using mass-scaled normal mode coordinates are given in atomic units ($1 \text{ a.u.} \simeq 0.0123943 \sqrt{\text{amu}} \text{ \AA}$). Relative displacements $\Delta = A_0^{1/2} \cdot \delta$, where A_0 is the width matrix of the initial wavepacket, are dimensionless and more appropriate measures of excitation since they take into account the fact that a displacement δ of low frequency mode has a smaller effect on the resulting spectrum than the same displacement δ of the high-frequency mode. Normal modes are ordered from the highest to the lowest ground-state frequency.

Mode	Symmetry	Ground state	Excited state AH			Excited state VH		
		ω cm^{-1}	ω cm^{-1}	δ a.u.	Δ	ω cm^{-1}	δ a.u.	Δ
1	a ₁	3193	3187	-0.06	-0.0054	3195	0.01	0.0007
2	b ₂	3184	3168	0	0	3166	0	0
3	a ₁	3181	3162	-0.14	-0.0122	3167	-0.04	-0.0032
4	b ₂	3168	3140	0	0	3155	0	0
5	a ₁	3161	3139	0.03	0.0025	3150	-0.02	-0.0017
6	b ₂	1631	1522	0	0	1548	0	0
7	a ₁	1573	1633	12.92	0.7732	1571	13.96	0.8357
8	a ₁	1468	1443	-9.41	-0.5442	1447	-10.39	-0.6007
9	b ₂	1460	1395	0	0	1494	0	0
10	b ₂	1336	1351	0	0	1364	0	0
11	b ₂	1303	1243	0	0	1273	0	0
12	a ₁	1172	1214	-3.39	-0.1749	1192	-3.36	-0.1890
13	b ₂	1171	1119	0	0	1090	0	0
14	b ₂	1069	1049	0	0	1037	0	0
15	a ₁	1047	1018	-11.51	-0.5623	1071	-9.87	-0.4820
16	a ₁	1015	1000	7.79	0.3745	1023	4.65	0.2237
17	b ₁	997	1027	0	0	1014	0	0
18	a ₁	981	924	30.81	1.4563	950	33.80	1.5977
19	a ₂	970	998	0	0	971	0	0
20	b ₁	895	968	0	0	934	0	0
21	a ₂	815	788	0	0	800	0	0
22	b ₁	721	768	0	0	696	0	0
23	a ₁	671	685	0	0	673	0	0
24	a ₁	614	590	-28.08	-1.0498	541	-39.27	-1.4682
25	b ₂	593	528	0	0	419	0	0
26	b ₁	425	355	0	0	223	0	0
27	a ₂	401	301	0	0	212	0	0

Benzene

Table S4: Bond lengths (in Å) at optimized geometries for ground (\tilde{X}^1A_{1g}) and first excited (\tilde{A}^1B_{2u}) states of benzene.

	\tilde{X}^1A_{1g}	\tilde{A}^1B_{2u}
R_{C-C}	1.398	1.430
R_{C-H}	1.086	1.085

Table S5: Derivatives of the transition dipole moment (in atomic units) of the benzene $\tilde{A}^1B_{2u} \leftarrow \tilde{X}^1A_{1g}$ electronic transition with respect to the normal mode coordinates associated with doubly-degenerate normal modes that transform as e_{2g} irreducible representation. These modes are called the *inducing modes*, as they are responsible for the observation of the formally symmetry-forbidden electronic transition in benzene. The strongest transitions are induced by the low-frequency modes 27 and 28, which exhibit the largest derivatives of the transition dipole moment. The molecule is oriented according to Mulliken’s convention (standard orientation): the axis of greatest symmetry is aligned with the z -axis, molecule lies in the xy plane, and the y -axis passes through two hydrogen and two carbon atoms. All elements of the transition dipole moment and its gradient that are not listed below are zero.

Mode	$\partial\mu_x/\partial q$	$\partial\mu_y/\partial q$	$\partial\mu_z/\partial q$
4	0.00055	-0.00265	0
5	-0.00207	-0.00071	0
7	-0.00002	-0.00242	0
8	0.00006	-0.00064	0
13	-0.00036	0.00067	0
14	0.00133	0.00018	0
27	0.00784	0.00235	0
28	0.00208	-0.00883	0

Table S6: Normal modes of benzene ground state with corresponding frequencies (in cm^{-1}), excited-state frequencies ω computed at the optimized ground-state geometry [vertical harmonic (VH) model] and optimized excited-state geometry [adiabatic harmonic (AH) model] (in cm^{-1}), displacements δ between the minima of the ground state and excited-state global harmonic potentials (in atomic units), and dimensionless relative displacements $\Delta = A_0^{1/2} \cdot \delta$. See the caption of Table S3 for details.

Mode	Symmetry	Ground state	Excited state AH			Excited state VH		
		ω cm^{-1}	ω cm^{-1}	δ a.u.	Δ	ω cm^{-1}	δ a.u.	Δ
1	a _{1g}	3207	3232	0.90	0.077	3212	0.87	0.074
2	e _{1u}	3197	3221	0	0	3199	0	0
3	e _{1u}	3197	3221	0	0	3199	0	0
4	e _{2g}	3182	3207	0	0	3183	0	0
5	e _{2g}	3182	3207	0	0	3183	0	0
6	b _{1u}	3172	3201	0	0	3177	0	0
7	e _{2g}	1642	1571	0	0	1678	0	0
8	e _{2g}	1642	1571	0	0	1678	0	0
9	e _{1u}	1515	1449	0	0	1497	0	0
10	e _{1u}	1515	1449	0	0	1497	0	0
11	a _{2g}	1378	1361	0	0	1385	0	0
12	b _{2u}	1353	1474	0	0	1620	0	0
13	e _{2g}	1198	1179	0	0	1215	0	0
14	e _{2g}	1198	1179	0	0	1215	0	0
15	b _{2u}	1176	1175	0	0	1201	0	0
16	e _{1u}	1061	970	0	0	1029	0	0
17	e _{1u}	1061	970	0	0	1029	0	0
18	b _{1u}	1017	999	0	0	1006	0	0
19	b _{2g}	1013	782	0	0	791	0	0
20	a _{1g}	1013	957	-21.28	-1.022	1035	-19.69	-0.946
21	e _{2u}	983	746	0	0	755	0	0
22	e _{2u}	983	746	0	0	755	0	0
23	e _{1g}	863	594	0	0	603	0	0
24	e _{1g}	863	594	0	0	603	0	0
25	b _{2g}	712	332	0	0	231	0	0
26	a _{2u}	689	555	0	0	577	0	0
27	e _{2g}	619	529	0	0	526	0	0
28	e _{2g}	619	529	0	0	526	0	0
29	e _{2u}	412	236	0	0	94	0	0
30	e _{2u}	412	236	0	0	94	0	0

Validation of the Born-Oppenheimer approximation

To justify the use of Born-Oppenheimer molecular dynamics, we consider the energy separation between the excited and ground electronic states as an indicator of crossings between the two surfaces. Figure S1 shows that the energy gap between the two electronic states is rather large during the propagation, implying the validity of the Born-Oppenheimer approximation. We note, however, that nonadiabatic couplings to the higher excited states could cause the breakdown of the Born-Oppenheimer approximation, especially in the case of the phenyl radical, where even the on-the-fly approach cannot reproduce the experimental spectrum perfectly. Finally, let us mention that the energy gap is only one of several criteria for determining the importance of nonadiabatic couplings. A more rigorous criterion monitors the population transfer and the most rigorous criterion monitors directly the *adiabaticity*, i.e., the fidelity between the Born-Oppenheimer and nonadiabatic wavefunctions.^{S5-S8}

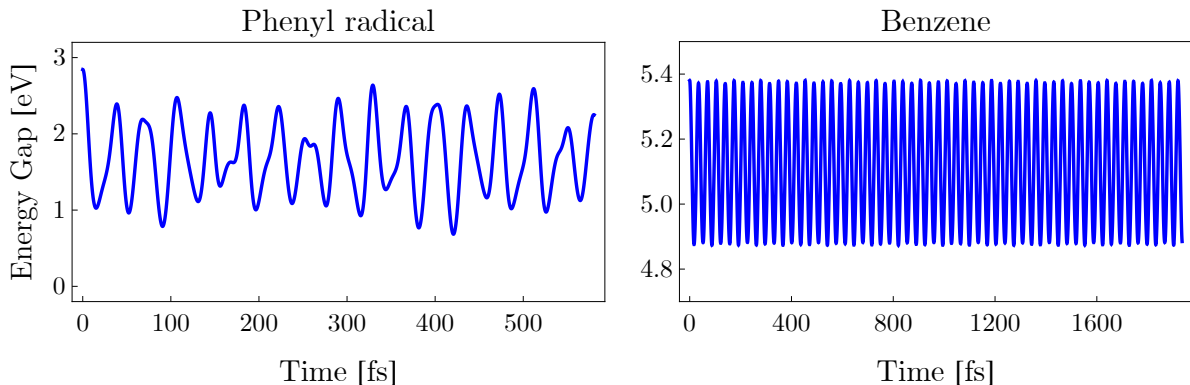


Figure S1: The energy gap between the excited and the ground electronic state for the phenyl radical (left) and benzene (right) evaluated along the *ab initio* trajectory.

Validation of the electronic structure method

To verify that the chosen electronic structure methods are reliable for benzene and the phenyl radical, we show the energies computed using the equation-of-motion coupled cluster (EOM-CCSD) method along the TDDFT trajectory (Fig. S2). Same basis sets were used as in the

TDDFT calculations: SNSD for the phenyl radical and 6-31+G(d,p) for benzene. The single point energy calculations were performed every 32 steps of the trajectory for the initial 200 fs. Although there is a shift in energy between the two methods, both give similar curvature of the potential energy surface. Our findings are in accord with the literature; indeed, B3LYP functional and the two basis sets have already been validated for spectra calculations of the phenyl radical and benzene by comparison with high-level electronic structure methods.^{S2,S9}

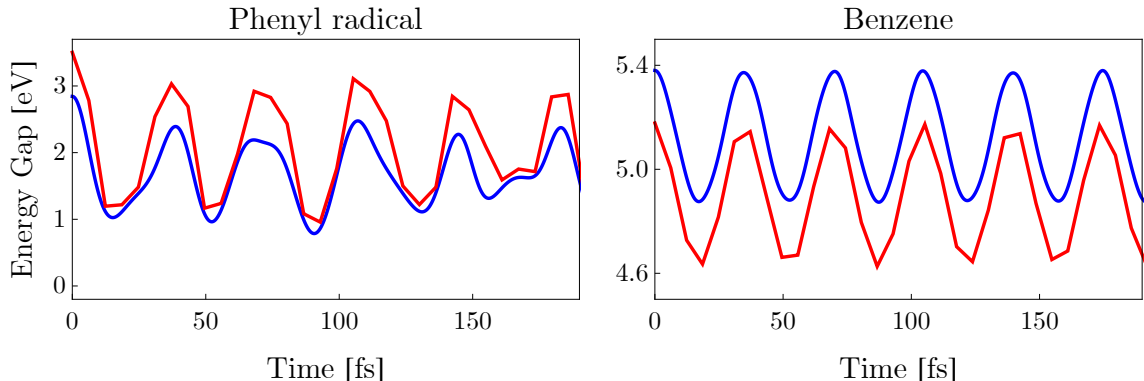


Figure S2: As in Fig. S1, but shown on a shorter time scale and compared to the energies computed using EOM-CCSD method (red).

Conservation of the phase space volume and symplectic structure

Classical dynamics preserves phase space volume. This statement, known as the Liouville theorem, is only one of D corollaries of the conservation of the symplectic structure, expressed by the equation

$$M_t^\top \cdot J \cdot M_t = J, \tag{1}$$

where M_t is the $2D \times 2D$ stability matrix evaluated at time t ,

$$J = \begin{pmatrix} 0 & I \\ -I & 0 \end{pmatrix} \tag{2}$$

is the standard symplectic matrix, I denotes the D -dimensional identity matrix, and D the number of degrees of freedom. The conservation of phase space volume, expressed by the condition

$$\det M_t = 1, \quad (3)$$

follows from Eq. (1). The fact that $\det M_t = \pm 1$ follows immediately by taking the determinant of both sides. Of the two options only $\det M_t = +1$ is possible since $\det M_0 = \det I_{2D} = +1$, since the determinant of a matrix is a continuous function, and since the stability matrix is a continuous function of time.

While our semiclassical propagation uses symplectic algorithms, the numerical implementation is performed at a finite precision; as a result, the conservation of symplectic structure and phase space volume are not guaranteed. However, monitoring their conservation provides a useful check of the semiclassical dynamics. Since the propagation of the thawed Gaussian wavepacket requires propagating the stability matrix, verifying the conservation laws is straightforward.

To check the symplectic condition (1), we monitor the Frobenius norm $\|\cdot\|_F$ of the difference $M_t^\top \cdot J \cdot M_t - J$; recall that the Frobenius norm of a general matrix A is defined as

$$\|A\|_F := \sqrt{\text{Tr}(A^\top \cdot A)}. \quad (4)$$

To check the conservation of phase space volume, we monitor $\det M_t$ and $\det(M_t^\top \cdot M_t)$ both of which should be equal to 1.^{S10} The time dependence of all three quantities is shown in Fig. S3, which confirms that our semiclassical dynamics conserves both phase space volume and symplectic structure within machine precision during the time that determines the spectra of benzene and the phenyl radical. Note, however, that even when the symplectic structure and phase space volume are not satisfied so accurately, it is possible to extend the semiclassical propagation time by regularizing the stability matrix.^{S11}

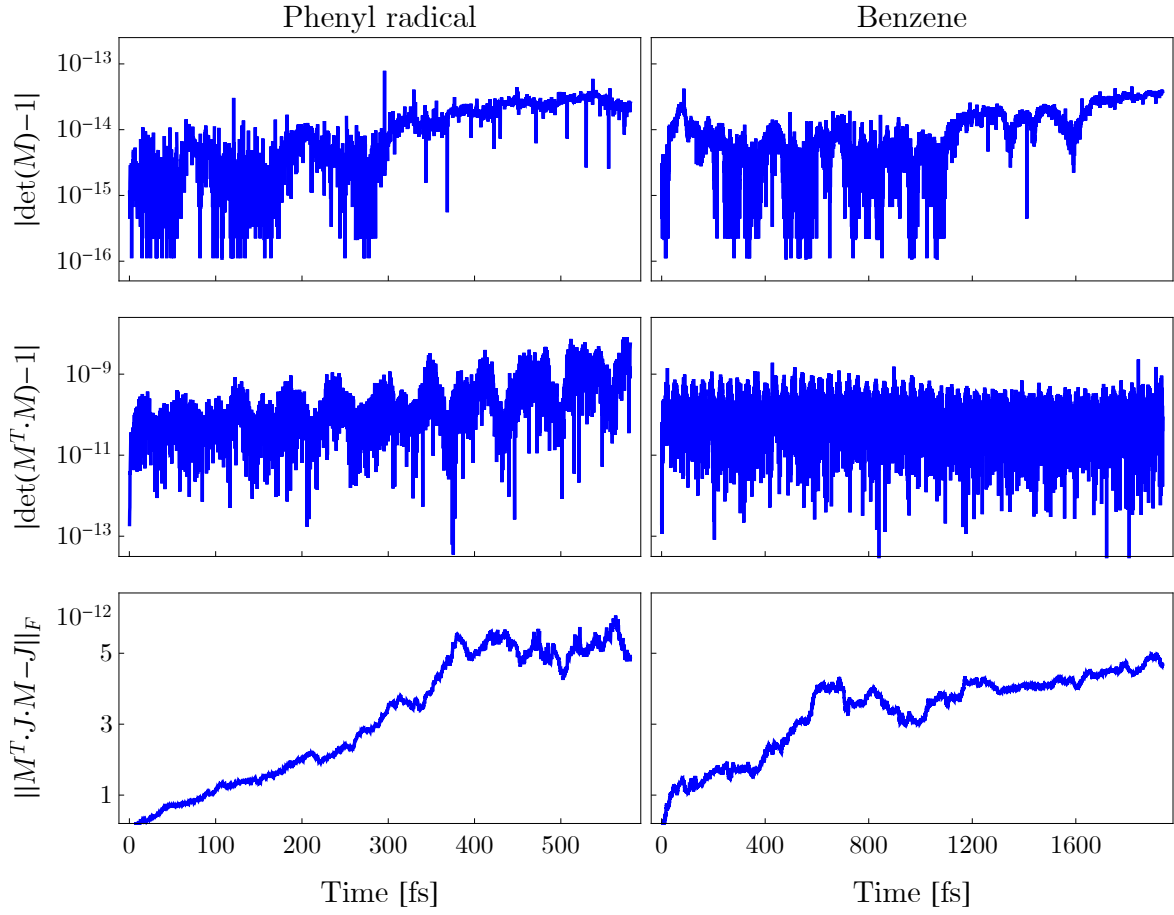


Figure S3: The errors in the determinant of the stability matrix (top panels), the determinant of $M^T \cdot M$ (middle panels), and the symplectic condition (bottom panels) for the phenyl radical (left) and benzene (right).

Horizontal shifts introduced into the calculated phenyl radical and benzene spectra

Table S7: Overall frequency shifts (in cm^{-1}) introduced into the calculated spectra of the phenyl radical and benzene. Same shifts were used for Franck-Condon, Franck-Condon Herzberg-Teller, and “Franck-Condon” spectra (see main text for definition).

	Phenyl radical	Benzene
OTF-AI	-437	3010
AH	-297	3020
VH	-267	3300

Models describing the failure of the vertical harmonic method for computing absorption spectra

Phenyl radical

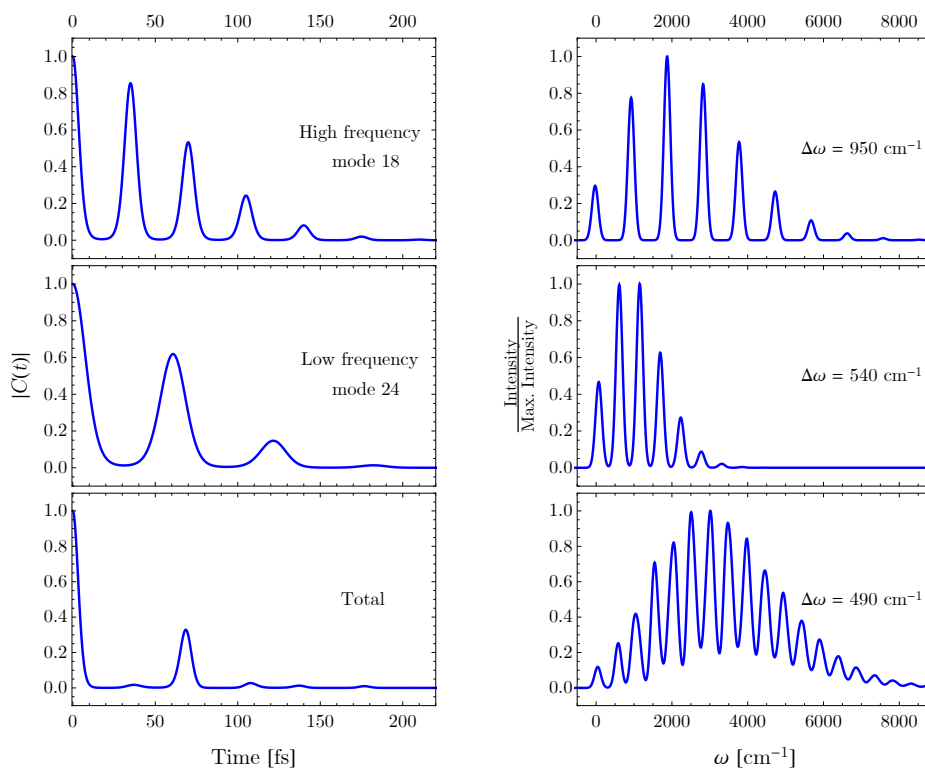


Figure S4: Autocorrelation functions (left panels) for a model system comprising two modes (mode 18 and mode 24) of the phenyl radical, and the corresponding spectra (right panels). The frequencies used correspond to the vertical harmonic model of the excited-state potential. When the modes are not coupled, the product of their autocorrelation functions represents the total autocorrelation function of the system, i.e., the autocorrelation function that would be obtained if a two-dimensional simulation were performed. It can be easily seen that the first small recurrence in the total autocorrelation function appears at a time that is different from any of the recurrences in the two one-dimensional cases. This is reflected in the corresponding spectra, each of which is showing a single progression. *While the spacings in the first two progressions are equal to the corresponding excited-state frequencies of the two modes, the overall spectrum contains only a single progression with a spacing of 490 cm⁻¹, resembling the situation observed in the vertical harmonic spectrum of the phenyl radical.* This value corresponds to neither of the two frequencies of the system and is called the *missing mode effect* frequency.

Benzene

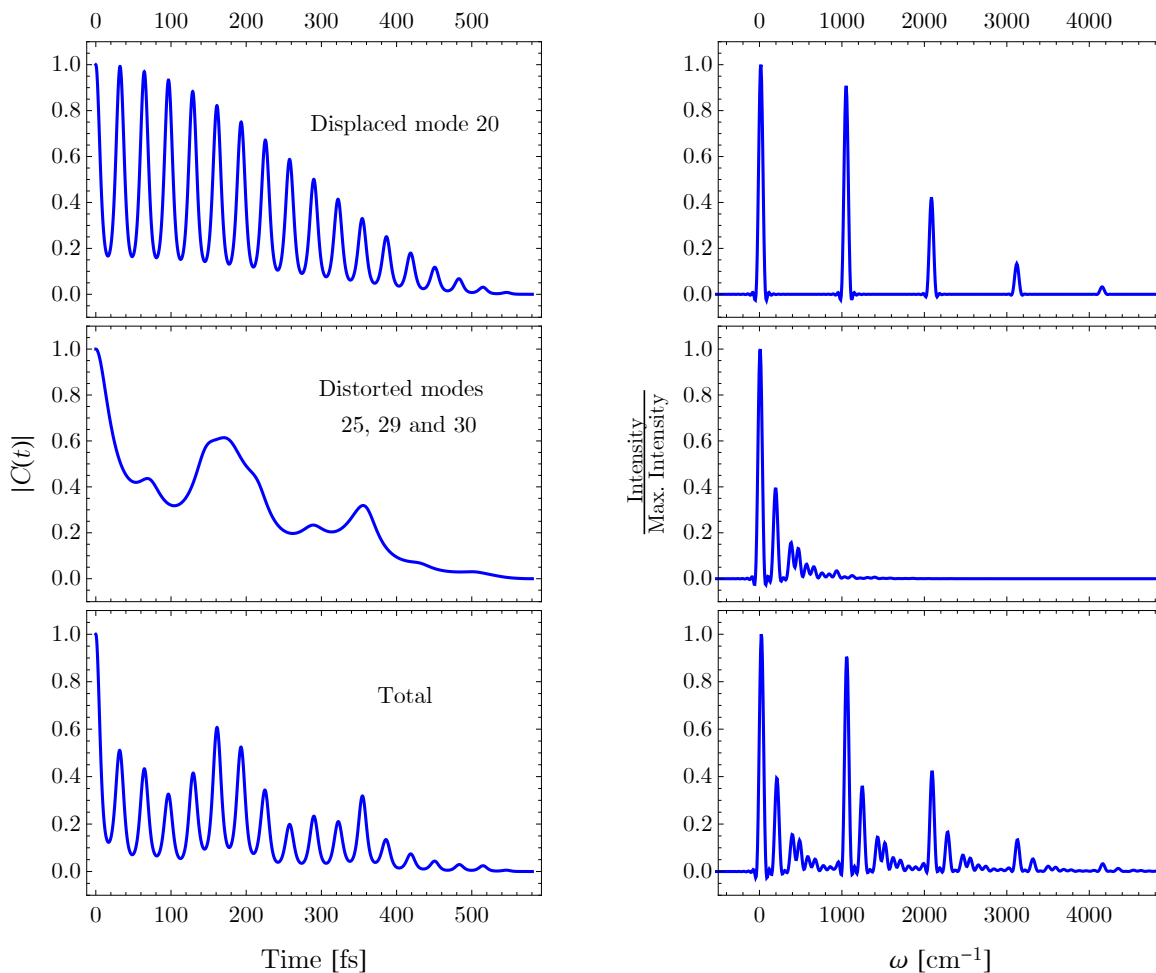


Figure S5: A four-dimensional model with three undisplaced highly distorted low-frequency modes, which correspond to benzene excited-state normal modes 25, 29 and 30, and one displaced mode, corresponding to the mode 20, is used to explain the observations in the vertical harmonic spectrum of benzene. The autocorrelation functions for the single displaced mode and the three distorted modes are given on the left, with the resulting spectra on the right. The total autocorrelation function (bottom, left) is the product of the two autocorrelation functions, and the corresponding spectrum is therefore a convolution of the two spectra in the frequency domain (bottom, right). *The resulting spectrum for this four-dimensional model is indeed similar to the observed VH spectrum and proves that overestimated distortions, i.e., incorrect low frequencies of the modes 25, 29 and 30, result in having more peaks than observed in the experimental spectrum.*

Anharmonicity effects in benzene

The VH model results in a qualitatively wrong absorption spectrum of benzene. In contrast, the static adiabatic harmonic picture is useful to describe the spectrum qualitatively, but does not provide correct intensities. A more dynamical picture is obtained by representing the vibrational motion in phase space. Significant dynamics is present only in the normal mode 20, whereas the other modes exhibit almost no classical dynamics. It is important to recall here *that the positions and momenta in the OTF approach result only from an on-the-fly ab initio classical dynamics on the excited state surface and do not depend on the accuracy of the excited-state Hessian calculations, while the dynamics in the global harmonic methods depends solely on the Hessian and the displacement of the excited-state potential.* This results in the differences observed in the phase space (see Fig. S6, top left).

The differences in the dynamics of the phase space center of the wavepacket can have strong effect on the resulting spectra, both in terms of the positions and the intensities of the peaks. In benzene, the phase-space dynamics in Fig. S6 reveals that the on-the-fly and adiabatic harmonic approaches are induced by different excited-state displacements of the normal mode 20. If the wrong displacement of the AH potential were the cause of poor spectral intensities, changing it to the value of the displacement of the OTF calculation would improve the spectrum. To test this hypothesis, a “modified” adiabatic harmonic potential is constructed by setting the displacement in the normal mode 20 to the displacement observed in the on-the-fly classical dynamics. However, this modified adiabatic potential yields a spectrum similar to the original one (see Fig. S6, bottom), even though the classical motion in the modified AH and OTF potentials energy surfaces are almost the same (Fig. S6, top right). *Thus, the difference in the classical dynamics is not the reason for the observed differences in the calculated spectra,* leaving the possibility that the differences in the spectra can only be explained by considering the width matrix and the phase of the wavepacket.

Although the classical dynamics is not affected by the anharmonicity of the excited-state potential, resulting in equally spaced peaks in the spectra, the intensities of the peaks are

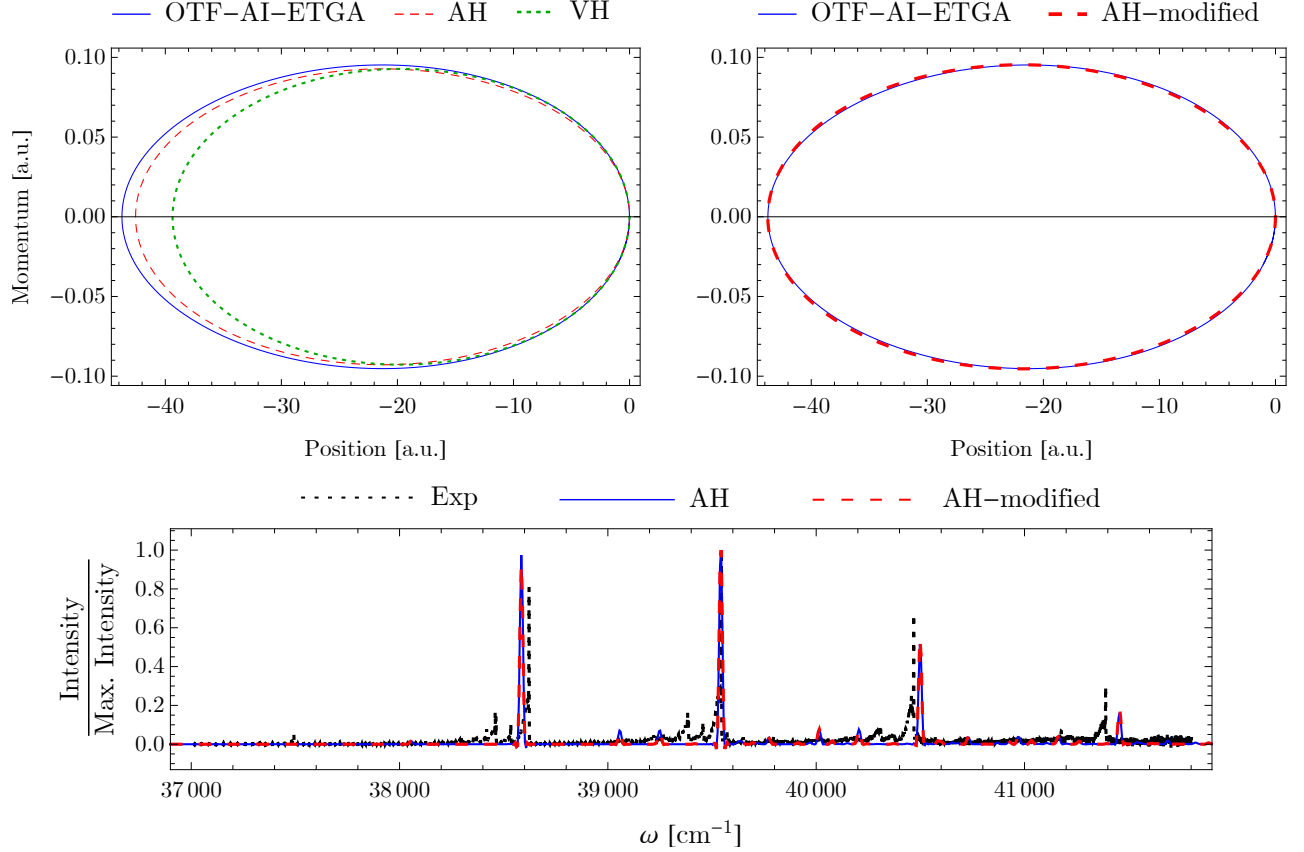


Figure S6: Phase-space representation of the dynamics in the normal mode 20 of benzene (top panels) and the spectrum (bottom panel) obtained using a modified adiabatic harmonic potential (AH-modified). Position and momentum are given in the mass-scaled normal mode coordinates in atomic units ($1 \text{ a.u.} \simeq 0.0123943 \sqrt{\text{amu}} \text{ \AA}$ for position and $1 \text{ a.u.} \simeq 0.512396 \sqrt{\text{amu}} \text{ \AA/fs}$ for momentum). The top left panel shows trajectories corresponding to three different methods—the on-the-fly, adiabatic harmonic, and vertical harmonic propagations, while the top right panel compares the on-the-fly classical dynamics with the dynamics in the modified adiabatic harmonic potential, i.e., the potential obtained by setting the displacement of the adiabatic harmonic potential in the normal mode coordinate 20 to the displacement observed in the OTF-AI dynamics. The AH-modified spectrum is compared to the original AH and experimental spectra in the bottom panel. Despite the similarity between the on-the-fly dynamics and the dynamics in the AH-modified potential (top right panel), the modified adiabatic harmonic spectrum shows no significant improvement over the original AH spectrum.

influenced by the changes in the autocorrelation function (Fig. S7). Such pattern in the relative intensities cannot be described by a simple global harmonic approach, but requires a method that can treat anharmonicity. The agreement with the experimental spectrum proves that running an on-the-fly trajectory with Hessians evaluated along the trajectory gives a reliable wavepacket propagation and accounts for fine details in the autocorrelation function.

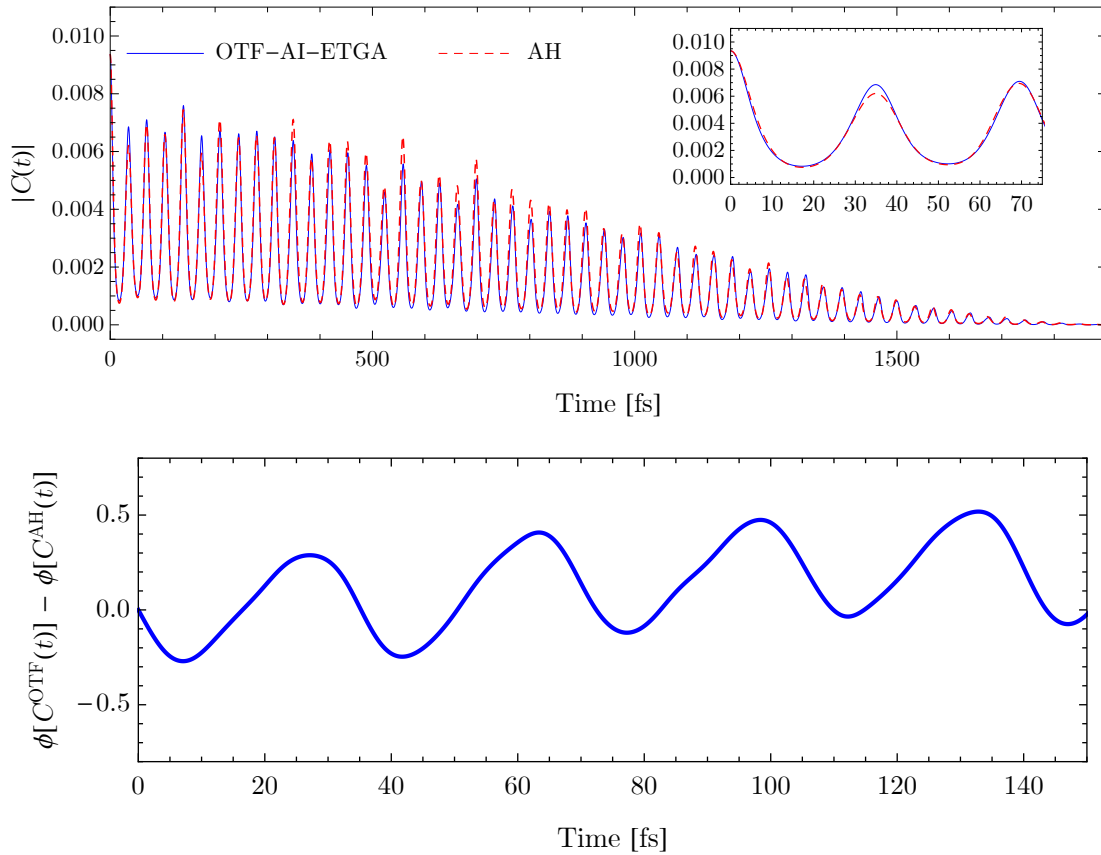


Figure S7: Autocorrelation functions calculated using the on-the-fly and adiabatic harmonic approaches are compared: the absolute values are shown in the top panel, while the difference of the phases on a shorter timescale is given in the bottom panel. Only slight differences in the shapes of the recurrences are observed in the magnitudes of the autocorrelation functions, while the difference of the phases is significant.

To further investigate the differences between the adiabatic harmonic approximation and the OTF-AI-ETGA, we explore the dynamics in the most active totally symmetric normal mode 20. Vertical and adiabatic harmonic Hessians yield different frequencies of this mode

and both approaches (see Table S6) propagate the wavepacket using only one value for the frequency of the mode (by definition, since they both use global harmonic potentials). However, the true potential is not perfectly harmonic. *The stiffness of the mode 20 changes along the trajectory, with the vertical Hessian representing the maximum and the adiabatic Hessian giving a value roughly equal to the mean frequency (see Fig. S8), explaining the better agreement of the AH with the OTF approach.*

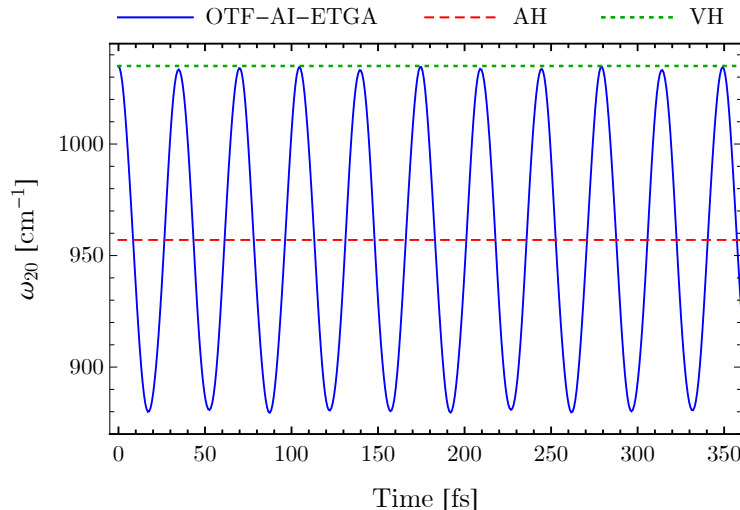


Figure S8: Frequency of the normal mode 20 of benzene in the excited electronic state as a function of time. Comparison of the on-the-fly, adiabatic harmonic, and vertical harmonic approaches.

“Franck-Condon” (“FC”) spectrum and absolute absorption cross sections of benzene

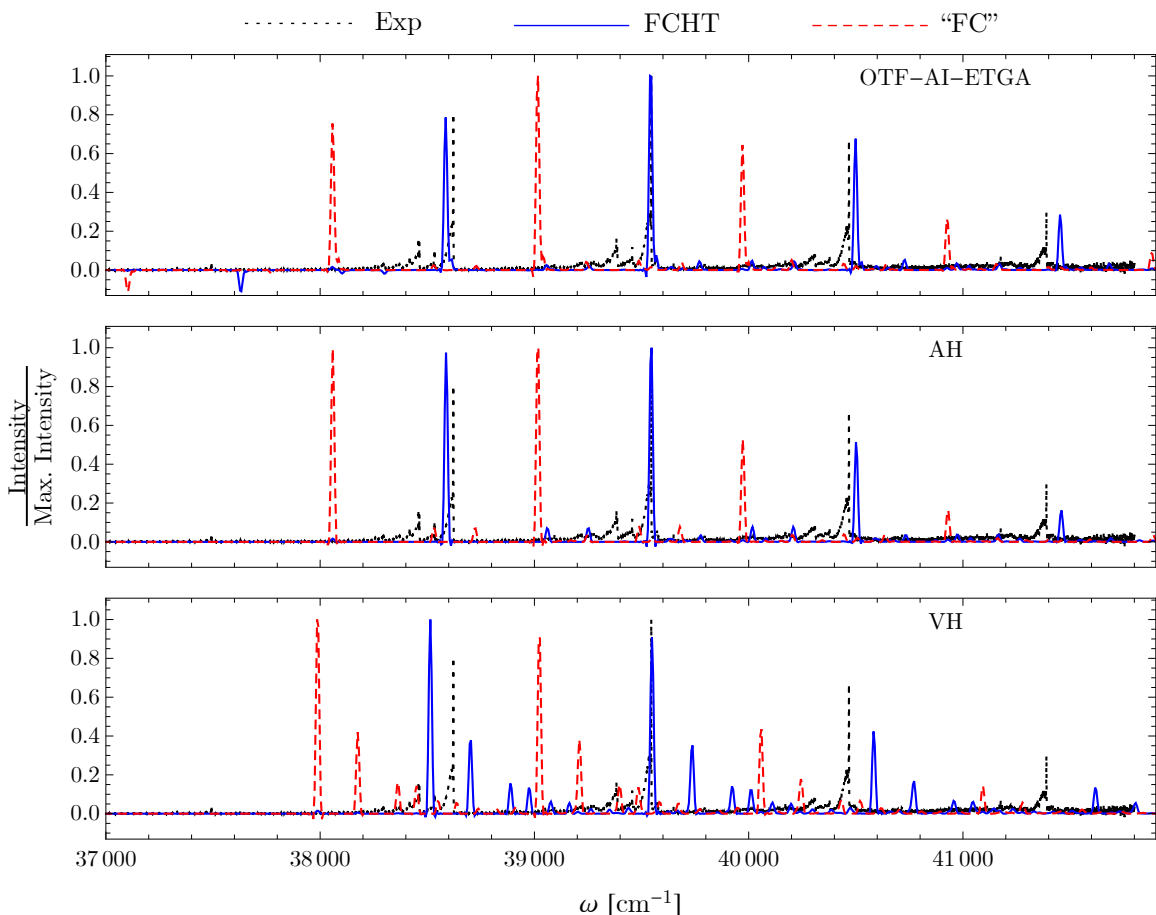


Figure S9: “FC” and FCHT spectra of benzene evaluated using the adiabatic harmonic (AH), vertical harmonic (VH), and on-the-fly *ab initio* extended TGA (OTF-AI-ETGA) approaches are compared with the experimental spectrum. All spectra were horizontally shifted and scaled according to the highest peak of the FCHT calculated spectra (see Table S7). The same horizontal shift for both “FC” and FCHT spectra was used as to show that the constant horizontal shift between them corresponds to the excited-state frequency of the inducing modes 27 and 28: $\omega = 529 \text{ cm}^{-1}$ for the AH, $\omega = 526 \text{ cm}^{-1}$ for the VH model.

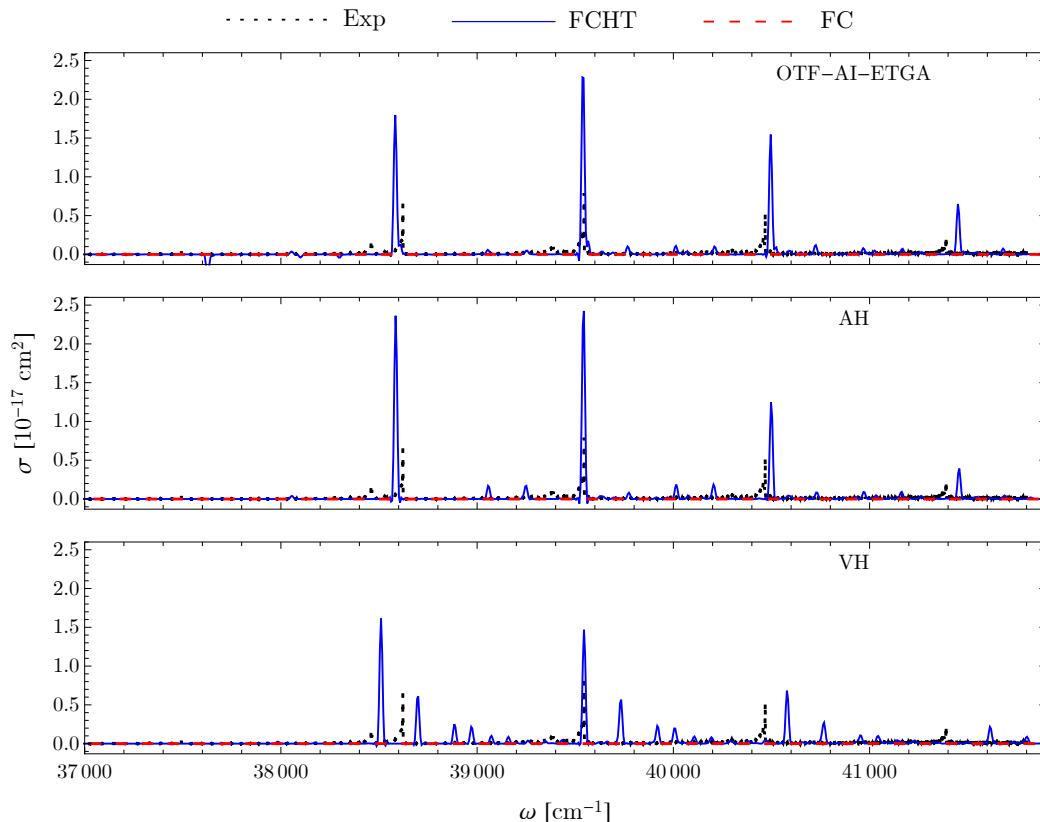


Figure S10: Absolute absorption cross sections, evaluated with the on-the-fly and global harmonic approaches, are compared to the experimental spectrum. The calculated spectra were horizontally shifted as in Fig. S9, but the magnitudes were not scaled. While the FC spectra are zero, because the transition dipole moment is zero, the spectra computed within the Herzberg-Teller approximation (FCHT) are in fair agreement with the experiment, although significantly overestimating the experimental values by a roughly constant systematic factor of ≈ 3 .

References

- (S1) Frisch, M. J.; Trucks, G. W.; Schlegel, H. B.; Scuseria, G. E.; Robb, M. A.; Cheeseman, J. R.; Scalmani, G.; Barone, V.; Mennucci, B.; Petersson, G. A.; Nakatsuji, H.; Caricato, M.; Li, X.; Hratchian, H. P.; Izmaylov, A. F.; Bloino, J.; Zheng, G.; Sonnenberg, J. L.; Hada, M.; Ehara, M.; Toyota, K.; Fukuda, R.; Hasegawa, J.; Ishida, M.; Nakajima, T.; Honda, Y.; Kitao, O.; Nakai, H.; Vreven, T.; Montgomery, J. A., Jr.; Peralta, J. E.; Ogliaro, F.; Bearpark, M.; Heyd, J. J.; Brothers, E.; Kudin, K. N.;

Staroverov, V. N.; Kobayashi, R.; Normand, J.; Raghavachari, K.; Rendell, A.; Burant, J. C.; Iyengar, S. S.; Tomasi, J.; Cossi, M.; Rega, N.; Millam, J. M.; Klene, M.; Knox, J. E.; Cross, J. B.; Bakken, V.; Adamo, C.; Jaramillo, J.; Gomperts, R.; Stratmann, R. E.; Yazyev, O.; Austin, A. J.; Cammi, R.; Pomelli, C.; Ochterski, J. W.; Martin, R. L.; Morokuma, K.; Zakrzewski, V. G.; Voth, G. A.; Salvador, P.; Dannenberg, J. J.; Dapprich, S.; Daniels, A. D.; Farkas, O.; Foresman, J. B.; Ortiz, J. V.; Cioslowski, J.; Fox, D. J. Gaussian 09 Revision D.01. Gaussian Inc. Wallingford CT 2009.

- (S2) Baiardi, A.; Bloino, J.; Barone, V. General Time Dependent Approach to Vibronic Spectroscopy Including Franck-Condon, Herzberg-Teller, and Duschinsky Effects. *J. Chem. Theory Comput.* **2013**, *9*, 4097–4115.
- (S3) Wehrle, M.; Šulc, M.; Vaníček, J. On-the-fly Ab Initio Semiclassical Dynamics: Identifying Degrees of Freedom Essential for Emission Spectra of Oligothiophenes. *J. Chem. Phys.* **2014**, *140*, 244114.
- (S4) Wehrle, M.; Oberli, S.; Vaníček, J. On-the-fly Ab Initio Semiclassical Dynamics of Floppy Molecules: Absorption and Photoelectron Spectra of Ammonia. *J. Phys. Chem. A* **2015**, *119*, 5685.
- (S5) Zimmermann, T.; Vaníček, J. Communications: Evaluation of the nondiabaticity of quantum molecular dynamics with the dephasing representation of quantum fidelity. *J. Chem. Phys.* **2010**, *132*, 241101.
- (S6) Zimmermann, T.; Vaníček, J. Measuring nonadiabaticity of molecular quantum dynamics with quantum fidelity and with its efficient semiclassical approximation. *J. Chem. Phys.* **2012**, *136*, 094106.
- (S7) Zimmermann, T.; Vaníček, J. Evaluation of the importance of spin-orbit couplings

- in the nonadiabatic quantum dynamics with quantum fidelity and with its efficient “on-the-fly” ab initio semiclassical approximation. *J. Chem. Phys.* **2012**, *137*, 22A516.
- (S8) Bircher, M. P.; Liberatore, E.; Browning, N. J.; Brickel, S.; Hofmann, C.; Patoz, A.; Unke, O. T.; Zimmermann, T.; Chergui, M.; Hamm, P.; Keller, U.; Meuwly, M.; Woerner, H. J.; Vaníček, J.; Rothlisberger, U. Nonadiabatic effects in electronic and nuclear dynamics. *Struct. Dyn.* **2017**, *4*.
- (S9) Li, J.; Lin, C.-K.; Li, X. Y.; Zhu, C. Y.; Lin, S. H. Symmetry Forbidden Vibronic Spectra and Internal Conversion in Benzene. *Phys. Chem. Chem. Phys.* **2010**, *12*, 14967–76.
- (S10) Zhuang, Y.; Siebert, M. R.; Hase, W. L.; Kay, K. G.; Ceotto, M. Evaluating the accuracy of Hessian approximations for direct dynamics simulations. *J. Chem. Theory Comput.* **2013**, *9*, 54–64.
- (S11) Di Liberto, G.; Ceotto, M. The importance of the pre-exponential factor in semiclassical molecular dynamics. *J. Chem. Phys.* **2016**, *145*, 144107.